Chapter 4

In Situ Engineering and Characterization of Correlated Materials with Integrated OMBE–ARPES

Dawei Shen, Haifeng Yang and Zhengtai Liu

Additional information is available at the end of the chapter

http://dx.doi.org/10.5772/65711

Abstract

Oxide molecular beam epitaxy has emerged as an effective technique to fabricate complex oxide thin films and novel superlattices with atomic-level precision. In this chapter, we first briefly introduce the oxide molecular beam epitaxy technique and then show how to use this technique to achieve high-quality thin films with good stoichiometry. Moreover, we exhibit that the combination of oxide molecular beam epitaxy and *in situ* angle-resolved photoemission spectroscopy is indeed a versatile toolkit to tailor and characterize properties of novel quantum materials.

Keywords: oxide molecular beam epitaxy (OMBE), correlated materials, angle-resolved photoemission spectroscopy (ARPES)

1. Introduction

In transition metal oxides, the subtle interplay among charge, orbital, lattice and spin degrees of freedom gives rise to a spectrum of fascinating physical phenomena, including high-temperature superconductivity [1], metal-insulator transition [2], colossal magnetoresistance [3], and so on. Remarkably, in thin film interfaces and ultrathin films of correlated oxides, emergent physics, which does not exist in bulk crystals, occurs [4, 5]. As a well-known example, two-dimensional electron gas with high mobility amazingly emerges at the interface of two-band insulators $LaAlO_3$ and $SrTiO_3$ [6]. This emergent electron gas was even found to be superconducting [7]. Another example is that strong ferroelectricity and ferromagnetism were found in $EuTiO_3/DyScO_3$ superlattices [8]. As Nobel laureate Herbert Kroemer said that 'the interface is the device' [9], these emergent physics may potentially revolutionize our modern technologies.

In order to access these thin film-based physics, the first and most important step is to grow these oxide thin film structures with high quality. This needs exquisite control of growth, and usually is very challenging. In the past several decades, fortunately, reactive oxide molecular beam epitaxy (OMBE) has been proved to be an effective technique in the growth of some oxides with high quality, though being not easy [10–12]. Recently, the *in situ* combined system of OMBE and angle-resolved photoemission spectroscopy (ARPES) [13–17] have shown great potential in exploring intricate many-body physics based on oxide film structures, which further intensifies the power of OMBE.

In this chapter, we first present basics of OMBE technique. Then, we show how to grow high-quality films with good stoichiometry, and the power of the integrated OMBE-ARPES in studying and designing many-body interactions in complex oxides.

2. Basics of OMBE technique

MBE is a vacuum deposition technique in which well-defined thermal beams of atoms or molecules react at a crystalline surface to produce an epitaxial film. Originally, it was developed to fabricate GaAs and (Al, Ga)As films [18], and soon successfully expanded to other semiconductors as well as metals and insulators. In addition to molecular beams coming from individual heated element source, gas molecular may also be introduced into MBE. Including gas oxidants (e.g., oxygen or ozone) can make an OMBE, which is now applied to grow oxides [11, 12].

In 1985, Betts and Pitt began to use this technique to grow $LiNbO_3$ films [19]. Later, motivated by the discovery of high-temperature superconductivity, OMBE was used to grow complex cuprate thin films. Up to now, it has been broadly employed to fabricate a pool of oxides, including oxide superconductors (e.g., (Ba, K)BiO_3, (La, Sr)$_2CuO_4$, $Bi_2Sr_2Ca_{n-1}Cu_nO_{2n+4}$, etc.), ferroelectrics (e.g., $LiTaO_3$, $PbTiO_3$, etc.), ferromagnets (e.g., (La, Ca)MnO_3, EuO, etc.), multiferroics (e.g., $BiFeO_3$, $YMnO_3$, etc.) and superlattices of these phases [11, 12].

While conventional MBE growth occurs in an ultra-high vacuum, in OMBE growth the induction of active gas oxidants can pose new challenges in the instrumentation as well as the film growth [11, 17]. The presence of oxidant species requires the hardware to be necessarily compatible with an oxidizing environment, thus high-temperature components (e.g., heater filaments, effusion cells and substrate holders, etc.) need to be made of highly oxidant-resistive materials. Moreover, adequate pumping is needed to deal with the oxidant gas load. Furthermore, oxygen acts as another variable which needs to be optimized in the growth, and oxygen inside films is tricky to study and manipulate. In addition, the oxidants can oxidize the cell materials such that one cannot get well-controlled fluxes as planned during growth. These challenges make the use of OMBE in the growth of oxides less mature than the use of MBE in semiconductor growth [11].

Figure 1 shows the schematic of a typical OMBE system. Single-element evaporators are used to generate atomic beams for OMBE growth. Knudsen cells and crucibles are chosen for

http://dx.doi.org/10.5772/65711

elements with desired fluxes below 2000°C, while electron beam evaporators are adopted for refractory elements (e.g., tungsten, ruthenium and iridium) which require higher temperature to provide the fluxes necessary for the growth. The atomic beams impinge upon the substrate unless they are blocked by shutters which are positioned at the output end of each cell and remotely controlled by a computer. The utilization of shutters enables the elemental fluxes to be supplied to in a continuous or a sequential way. The fluxes can be adjusted by changing the cell temperature, and are *in situ* measured by a quartz crystal microbalance (QCM). Reflective high-energy electron diffraction (RHEED) is used in OMBE for the *in situ* characterization of the growing surface. Due to the grazing angle diffraction, it can provide surface-sensitive information including thin film crystallinity, roughness, in-plane lattice constants, growth mechanism and phase purity. If intermediate products or impurity phases are formed, the growth conditions would be adjusted accordingly. Distilled ozone was used as the oxidant. Compared to oxygen, ozone has stronger oxidizing ability and thus needs lower pressure.

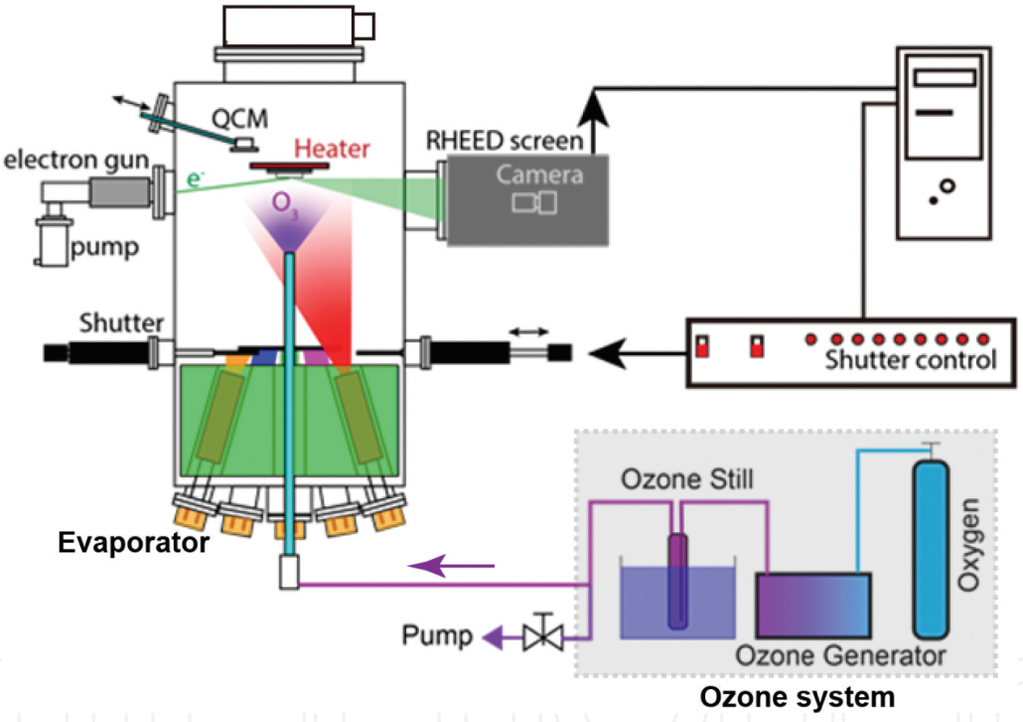

Figure 1. Schematic illustration of an OMBE system with an ozone-generating system. Reproduced with permission from Ref. [17].

Figure 2 displays the photo of DCA R450 OMBE system in Shanghai Institute of Microsystem and Information Technology (SIMIT). It is equipped with 10 changeable effusion cells, and one four-seat e-beam evaporator for at most four refractory elements, which can cover all transition metals of interests. It also has *in situ* QCM to measure the fluxes and real-time RHEED to directly monitor the growth. Ozone was obtained from self-made ozone-generating-and-distilling system. Ozone generator would generate a small amount of ozone out of oxygen gas, then silica gel cooled down with liquid nitrogen would absorb ozone. Warming up the silica gel would give out the ozone gas to be used in OMBE growth.

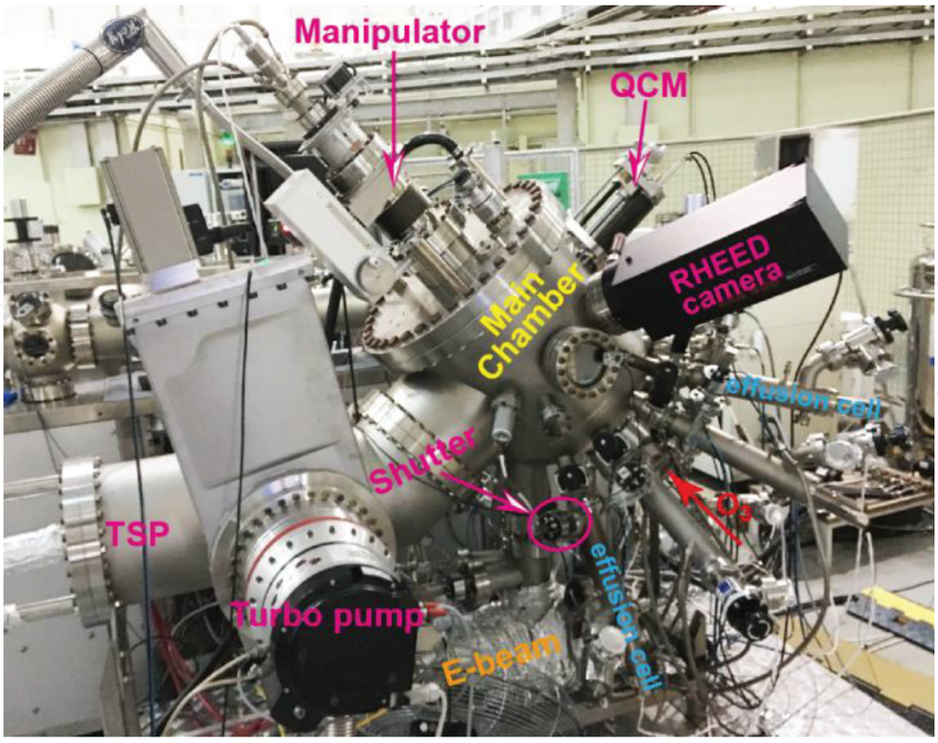

Figure 2. OMBE system in Shanghai Institute of Microsystem and Information Technology (SIMIT), Chinese Academy of Sciences.

3. Fabricating oxide thin films with good stoichiometry by OMBE

In this section, we show generally how to grow high-quality oxide thin film with good stoichiometry by OMBE. Starting with choosing the proper substrate, we mainly talk about two growth methods commonly used—absorption-controlled growth and shutter growth—to achieve high-quality films.

Epitaxial thin films cannot be obtained without using proper substrates. The substrate not only guides the growth of thin film with the right crystalline structure but also provides the knob of strain which can essentially tune the electronic structure of the material [20]. **Figure 3** displays lattice constants of single-crystalline perovskite substrates which are commercially available and commonly used to grow perovskite or layered perovskite oxide thin films. If growing $LaNiO_3$ films with a pseudo-cubic lattice constant of 3.84 Å on $LaAlO_3$ (3.75 Å) substrates, an in-plane compressive strain was applied; if using $SrTiO_3$ (3.905 Å) as the substrate, an in-plane tensile strain was applied. In addition to the strain, in some cases, the choice of the substrate is vital to obtain high-quality films. For example, Proffit et al. reported that (1 1 0) orthorhombic $CaRuO_3$ films grown on orthorhombic (1 1 0) $NdGaO_3$ substrates (symmetry matched) exhibit atomically smooth surfaces, whereas films on cubic lanthanum aluminate-strontium aluminium tantalate (LSAT) substrates (symmetry mismatched) show rather rough surfaces [21]. Another example is the film growth of $LaNiO_3$ with polar orientations. As polar discontinuity is suggested to induce surface reconstructions which further lead

http://dx.doi.org/10.5772/65711

to bad quality of films [22, 23], metallic Nb-doped $SrTiO_3$ and iso-polarity $LaAlO_3$ substrates were shown to be more suitable than the common $SrTiO_3$ in the growth of $LaNiO_3$ films [24].

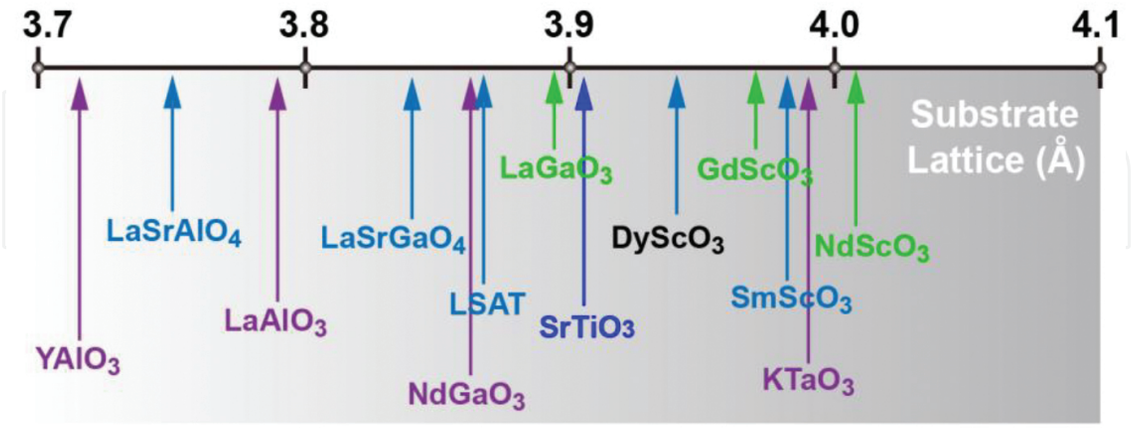

Figure 3. A number line showing the *a*-axis lattice constants in angstroms of the perovskite and perovskite-related substrates that are commercially available.

As illustrated above, the remotely controlled shutters in OMBE allow elemental fluxes to be supplied to in a continuous or a sequential way. Take the growth of perovskite ABO_3 (can be viewed as alternate stacking of AO and BO_2 layers along the (0 0 1) direction) as an example. As schematically shown in **Figure 4**, both shutters of A cell and B cell keeping open in the whole growth make a co-deposition growth. If the shutters of A cell and B cell alternately turn open (finishing the growth of one AO layer, and then starting the growth of one BO_2 layer), we can call this the shutter growth. In either growth, stoichiometry is the most important goal which needs to be achieved.

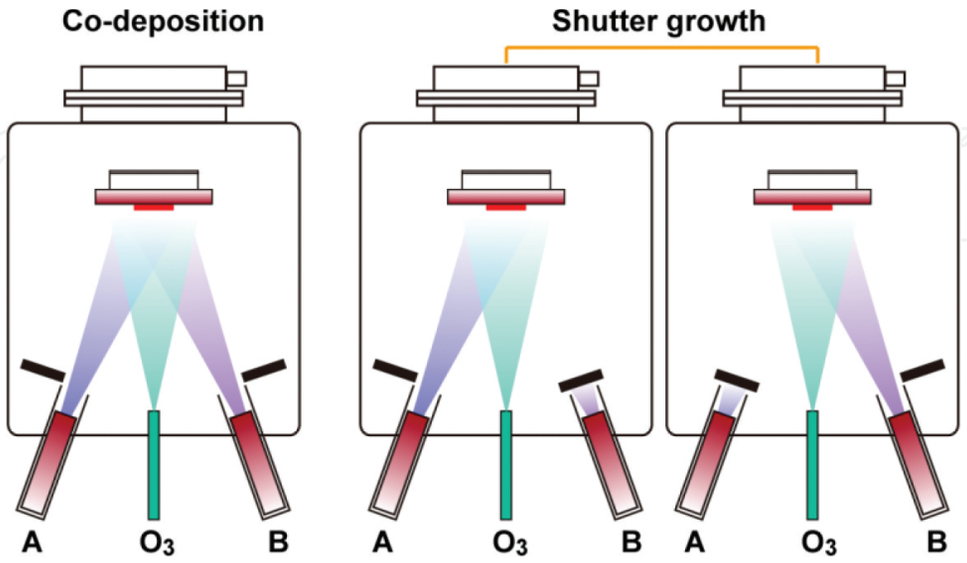

Figure 4. Schematics of co-deposition and shutter growth in OMBE growth.

A well-known growth method to achieve stoichiometric films is the adsorption-controlled growth, which was previously used to grow GaAs and recently has been used to fabricate several oxides such as $PbTiO_3$ [25], $BiFeO_3$ [26] and $BiMnO_3$ [27]. It is used in the growth of some compounds containing volatile species which can re-evaporate during growth while the others are less volatile. If always making this volatile species excess during the growth as well as optimizing the substrate temperature and oxygen partial pressure, stoichiometric growth can be conveniently achieved. Lee et al. reported the adsorption-controlled growth of $BiMnO_3$ in which the bismuth oxides are volatile [27]. **Figure 5** displays the calculated Ellingham diagram and obtained RHEED patterns [27]. The Bi:Mn flux ratio was fixed to be 3:1. Besides, the substrate temperature and oxygen partial pressure were fully explored to finally expose the growth window (see shadow region II in **Figure 5**) for phase-pure stoichiometric $BiMnO_3$ films which were verified by the shiny diffraction spots in the RHEED pattern.

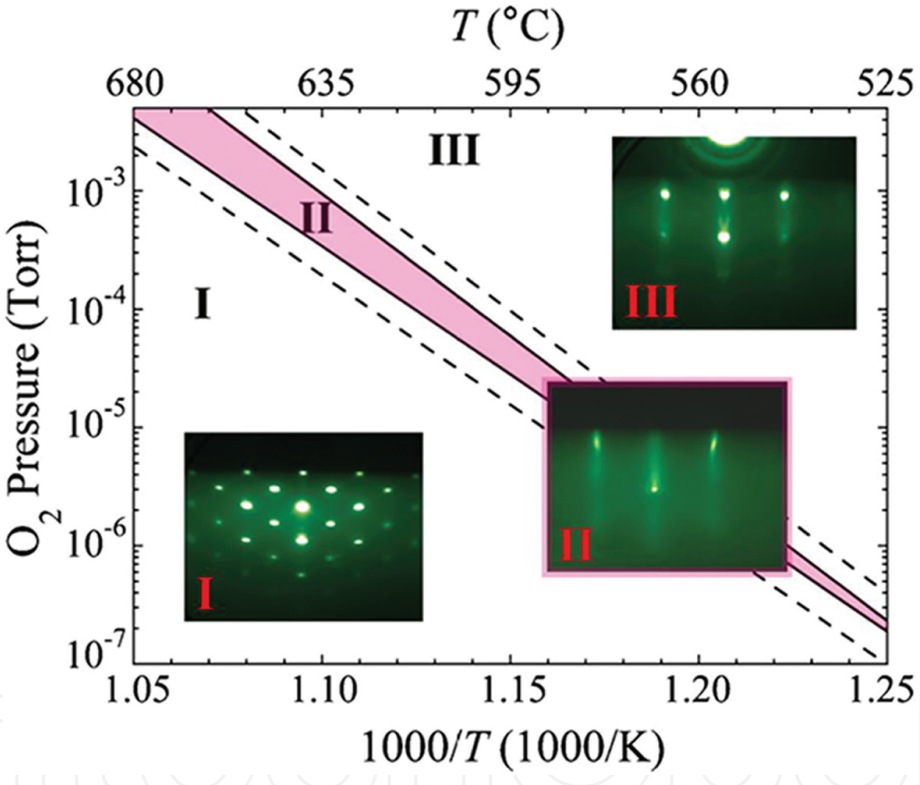

Figure 5. Calculated Ellingham diagram and RHEED patterns collected along the [1 1 0] azimuth of $SrTiO_3$ during the deposition of $BiMnO_3$ at different temperatures and oxygen partial pressures. Phase stability between Bi_xO_y gases and $BiMnO_3$ + Mn_3O_4, $BiMnO_3$ and $BiMnO_3$ + $Bi_2O_{2.5}$ condensed phases is represented by regions I, II and III, respectively. Reproduced with permission from Ref. [27].

For most oxides, adsorption-controlled growth unfortunately cannot be applied. To achieve good stoichiometry, generally, one has to adjust the deposition amount based on cycles of combined studies of QCM, RHEED patterns and oscillations, X-ray diffraction (XRD) pattern fitting, Rutherford backscattering spectroscopy, and so on. In the homo-epitaxial growth of $SrTiO_3$, Schlom's group reported the empirical method of optimizing shuttered RHEED oscillations to successfully achieve stoichiometric $SrTiO_3$ film within 1% composition deviation

http://dx.doi.org/10.5772/65711

[28, 29]. In the shutter growth of $SrTiO_3$, the intensity of diffraction spot would exhibit periodic oscillations at the pace of mechanically closing/opening shutters: in Ti doses, the intensity will decrease monotonically while in Sr doses the intensity will increase. It was shown that if oscillations exhibited smooth sinoidal shape with similar amplitude (**Figure 6(a)**), the resulted film was investigated to be stoichiometric [29]. If Sr is 10% excess, the combined feature of cusp and shoulder would show up (**Figure 6(b)**); if Sr is 10% deficient, the amplitude of individual oscillations would oscillate (**Figure 6(c)**). Thus, in growth, the real-time performance of RHEED oscillations would infer what to do next to achieve the stoichiometry [29].

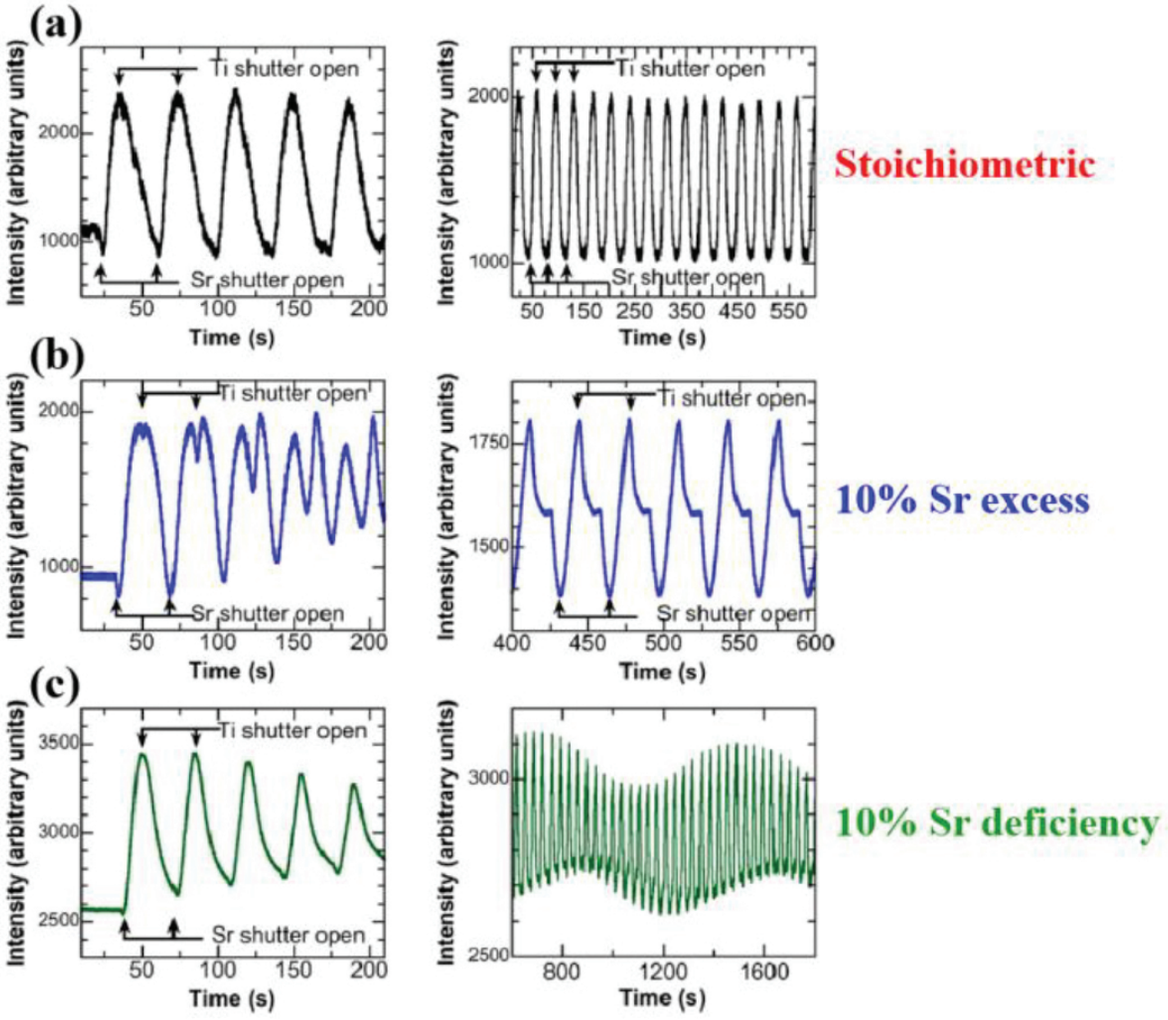

Figure 6. Shuttered RHEED oscillation behaviour of $Sr_{1+x}TiO_{3+\delta}$ films with stoichiometric (x = 0) (a), 10% strontium excess (x = 0.1) (b) and 10% strontium deficiency (x = -0.1) (c). Reproduced with permission from Ref. [29].

Compared to adsorption-controlled growth, shutter growth is a more straightforward way to control the film thickness and grow complex oxide structures such as Ruddlesden-Popper (RP) series $A_{n+1}B_nO_{3n+1}$ and various superlattices which display a wide range of physics. By conveniently changing the shuttering sequence of A and B ions to match the layering sequence of the desired RP phase, Haeni et al. and Tian et al. reported the OMBE growth of five RP members

of $Sr_{n+1}Ti_nO_{3n+1}$ [30] and $Sr_{n+1}Ru_nO_{3n+1}$ [31], respectively. Their structures with right-layering sequences were verified by high-resolution cross-sectional TEM measurements (**Figure 7**).

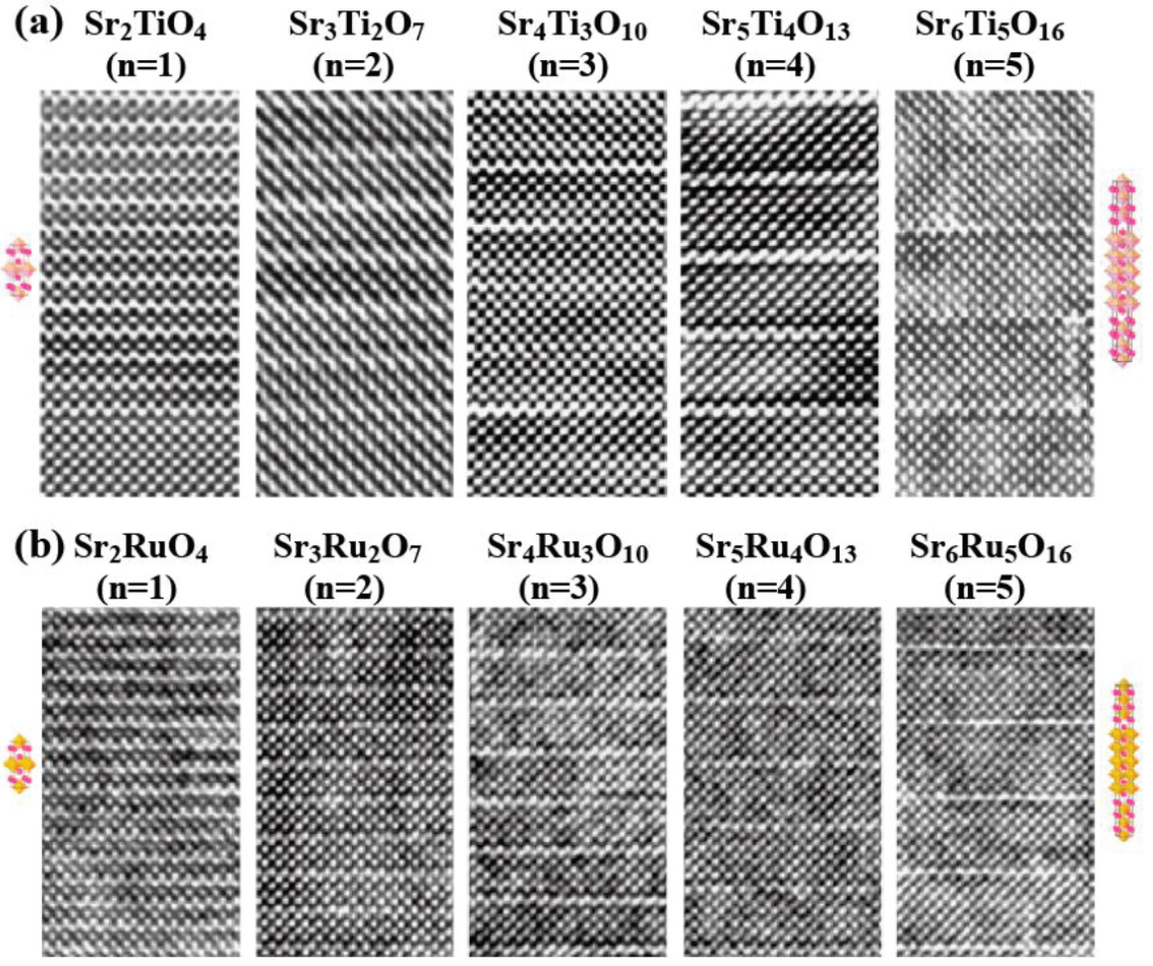

Figure 7. High-resolution cross-sectional TEM images of the same five members of the (a) $Sr_{n+1}Ti_nO_{3n+1}$ and (b) $Sr_{n+1}Ru_nO_{3n+1}$ Ruddlesden-Popper homologous series grown by OMBE. Reproduced with permission from Refs. [30] and [31].

4. The unique *in situ* combo of OMBE and ARPES

ARPES can directly visualize electronic band structures of solids, and therefore has emerged as an essential experimental technique to study various novel quantum materials such as superconductors and topological quantum materials [13, 14, 32]. It can be viewed as the 'k-space' microscope, and can provide the essential information about how electrons move inside the material. Based on the well-known photoelectric effect, an electron inside the solid can absorb an incident photon with a high enough energy and then emit out of the solid. If the kinetic and momentum of the photoelectrons are detected, the band structure of the material (as a function of binding energy and momentum) can be reconstructed in the context of

http://dx.doi.org/10.5772/65711

conversation laws and some reasonable assumptions, as shown in **Figure 8**. Generally being a surface-sensitive probe, ARPES demands clean and well-ordered sample surface, which is usually obtained by cleaving single crystals.

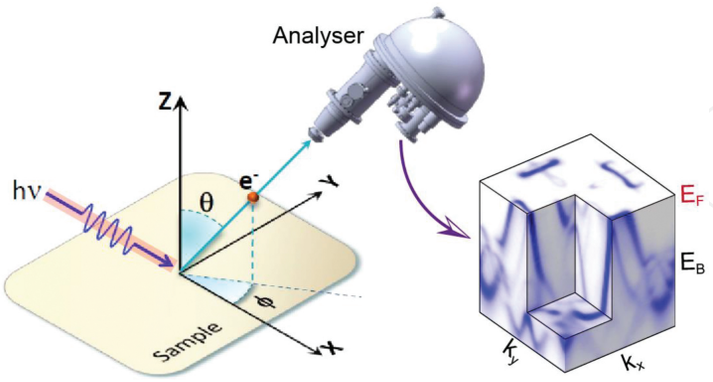

Figure 8. Schematic of ARPES measurement and the obtained band structure. Photoelectrons are emitted when shining the sample with light whose energy is larger than the sample work function. By using an electron analyser to pick up these electrons, we could obtain their energy and momentum information.

Recently, there has been increasing awareness that the *in situ* combo of OMBE and ARPES (ARPES is *in situ* connected to OMBE) could be a powerful approach in tailoring many-body interactions and uncovering the underlying physics of complex oxides. It is a win-win case: OMBE can provide high-quality thin films (especially those who cannot be cleaved properly in bulk form, e.g., perovskite oxides) and interesting superlattices, whose clean surfaces 'naturally' allow for the *in situ* ARPES studies; in return, ARPES can characterize the quality of these films which further give feedbacks to the growth, and moreover it can fully explore the band structures of films and study their intriguing physics [15–17, 33, 34].

Figure 9 shows the photo of such an *in situ* combo system located in Shanghai Institute of Microsystem and Information Technology (SIMIT), Chinese Academy of Sciences. A transfer chamber with high vacuum (~10×10^{-10} Torr) is used to bridge the OMBE system and ARPES

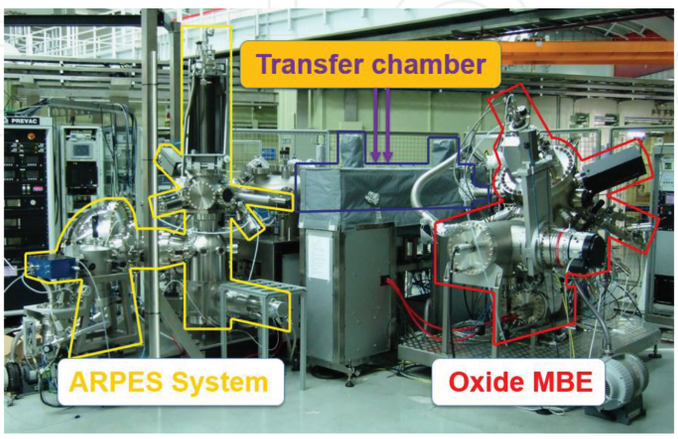

Figure 9. A photo of the *in situ* combo of OMBE and ARPES system in Shanghai Institute of Microsystem and Information Technology (SIMIT), Chinese Academy of Sciences.

system. Once the growth was finished, the film was immediately transferred to the ARPES chamber within 5 min through the transfer chamber. In so doing, the clean sample surface is expected to be preserved for ARPES studies.

Below, we first present studies on ultrathin perovskite $LaNiO_3$ films (*3d* system) [16], $SrRuO_3$ films (*4d* system) [35] and $SrIrO_3$ films (*5d* system) [36] of which the bulk form lacks natural cleaving planes, as examples to show the power of this *in situ* combo in studying the many-body interactions of complex oxides. Generally, when going from *3d* to *5d* elements, Coulomb interactions among electrons would increase as electrons are more and more delocalized, while the spin-orbital coupling (SOC) would become stronger due to the heavier elements. Then, we show the studies on $(LaMnO_3)_{2n}/(SrMnO_3)_n$ superlattices [17].

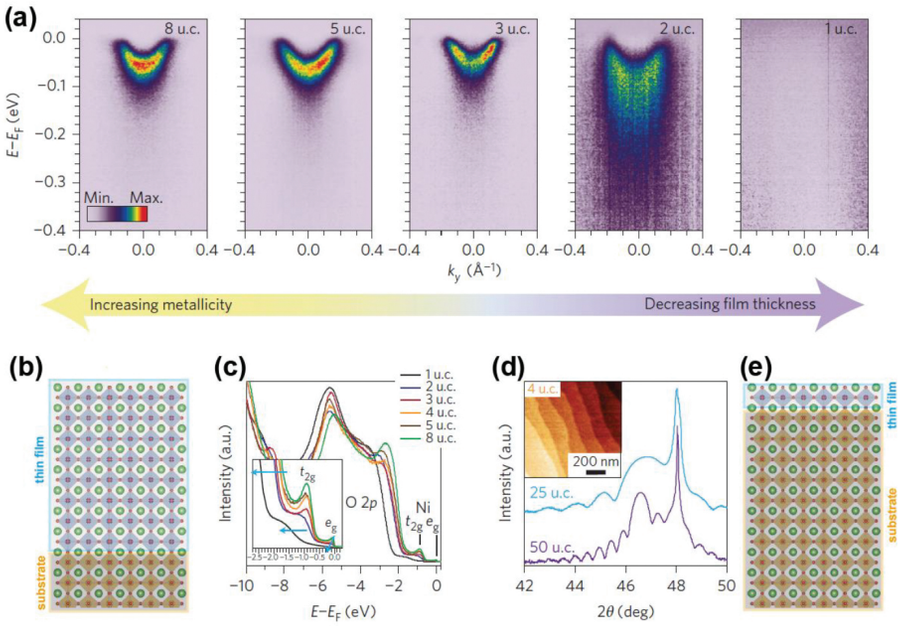

Figure 10. Metal-insulator transition in ultra-thin $LaNiO_3$ films. (a) The evolution of the electronic structure across the metal-insulator transition with decreasing the $LaNiO_3$ film thickness. (b) Schematic of 8-UC-thick $LaNiO_3$ film on $LaAlO_3$ substrate. (c) Angle-integrated photoemission spectroscopy along ($0.5\pi/a$, $0.7\pi/a$) of films varying from 8-UC-thick to 1-UC-thick. The inset shows the near-E_F angle-integrated spectra. (d) X-ray diffraction and atomic force microscopy results. (e) Schematic of 1-UC-thick $LaNiO_3$ film on $LaAlO_3$. Reproduced with permission from Ref. [16].

Bulk $LaNiO_3$, though being strongly correlated with $3d^7$ configuration of Ni^{3+}, remains a paramagnetic metal at low temperatures. By means of OMBE, King et al. synthesized atomically defined layers of $LaNiO_3$ films down to just one unit cell (UC) thickness, and observed an abrupt metal-insulator transition in 2-UC-thick film by transport studies [16]. The high quality of the films with atomically flat surfaces was revealed by the Kiessig fringes in XRD patterns and atomic force microscope image (**Figure 10(d)**). Then, *in situ* ARPES studies were carried out to investigate the competing electronic phases while crossing the transition, as shown in **Figure 10(a)** and **(c)**. The bulk-like electronic structure and Fermi liquid characteristics were found to remain almost unaffected by film thickness down to 3 UC (all exhibiting similar electron pocket), which is in contrast to the previous reports that an insulating state

http://dx.doi.org/10.5772/65711

emerged in 5-UC thickness or above and again reflects the high quality of the films. This makes 3-UC-thick LNO the thinnest metallic nickelate reported. Reducing the thickness by just one further UC (2 UC), however, causes the spectral weight near E_F to be suddenly suppressed. For 1-UC-thick $LaNiO_3$ film, no spectral weight was observed at E_F, indicative of a full-charge gap. This evolution was also observed in angle-integrated photoemission spectra. The authors claimed that the metal-insulator transition is driven by instability to an incipient order of the underlying quantum many-body interactions, and demonstrated the power of artificial confinement to harness control over competing phases in complex oxides with atomic-scale precision [16].

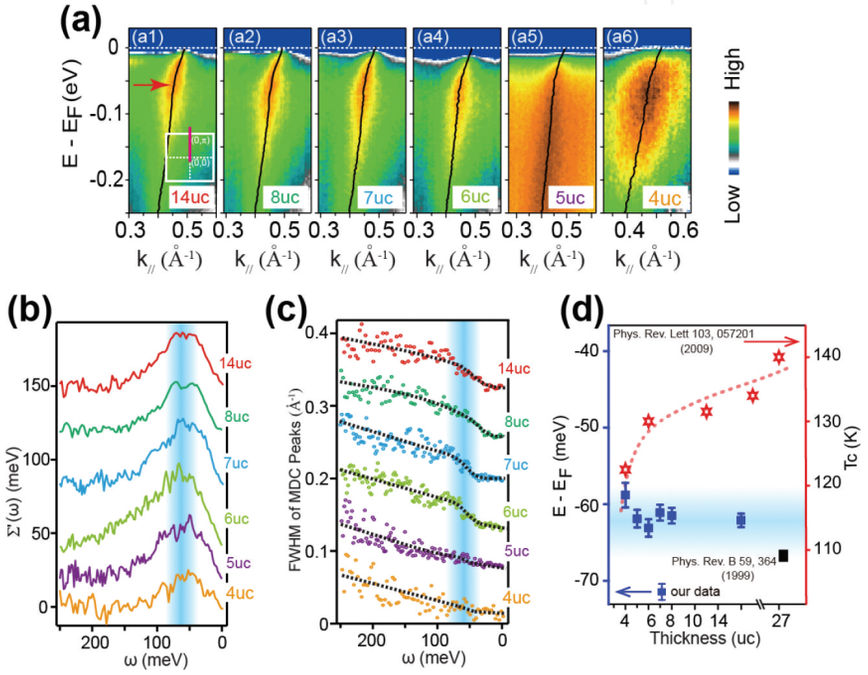

Figure 11. Electron-phonon coupling origin of the kink in the dispersion of $SrRuO_3$. (a) The evolution of the electronic structure of $SrRuO_3$ film with reducing the thickness. The kink persists in all films down to 4-UC thick. (b) and (c) Real part and imaginary part analyses of self-energies. All kinks occur at around 62 meV below E_F. (d) Electron-phonon coupling origin of the kink in $SrRuO_3$ films. Left axis: measured negligible thickness dependence of the kink energy. Right axis: reported thickness dependence of the Curie temperature. The black rectangular marker displays the energy scale of in-phase-stretching phonon mode proposed by the combined studies of Raman spectroscopy and calculation. Reproduced with permission from Ref. [35].

Perovskite $SrRuO_3$, a prototypical conductive ferromagnetic oxide, exhibits a kink in its band dispersion signalling the unusual electron dynamics therein [34]. The kink could originate from electron-magnon coupling or electron-phonon coupling. Uncovering the origin of this kink would hint on the studies of kinks' origins in many other intriguing systems [37–39] including the cuprate superconductor family [40]. Yang et al. reported the systematic thickness-dependent electronic structure studies on $SrRuO_3$ films with well-controlled thicknesses by using the OMBE and ARPES system [35]. **Figure 11(a)** shows the evolution of band dispersions of $SrRuO_3$ films with reducing the film thickness. Evidently, in all these spectra, the slope of the dispersion near E_F is markedly smaller than that of high-binding-energy region, namely

the kink persists even down to 4-UC-thick film. Empirical self energy analyses were carried out to determine the kink energy. As shown in **Figure 11(b)** and **(c)**, both real part and imaginary part analyses reveal that all films' kinks are around 62 meV below E_F. This is in sharp contrast to the report that reducing the thickness would decrease the Curie temperature [41], which implies that electron-magnon should not play a dominant role. On the other hand, the kink energy matches that of in-phase-stretching phonon mode proposed by the combined studies of Raman spectroscopy and calculation [42]. Thus, electron-phonon coupling should mainly contribute to this kink. This work can serve as an example to study the low-energy excitations of complex oxides.

Perovskite $SrIrO_3$, due to the heavy element of Ir, is expected to have strong SOC which is the key ingredient in building topological quantum materials [43, 44]. Therefore, novel topological phases were proposed in artificial $SrIrO_3$-based structures [45]. In particular, $SrIrO_3$ was proposed to be an exotic semimetal induced by the delicate interplay between SOC and electron correlations, in which a Dirac nodal ring near the *U* point would render a non-trivial topological semi-metallic state [46, 47]. Based on the OMBE-ARPES combo, Liu et al. synthesized high-quality $SrIrO_3$ films, and investigated its low-lying electronic structure [36]. **Figure 12** displays the measured band structure of $SrIrO_3$. In addition to the semimetal state (the Fermi level simultaneously crosses the hole and electron pockets), near the *U* point, a lifted Dirac node was directly observed, which agrees well with the authors' calculations. This Dirac node lifting could be due to the selectively breaking of *n*-glide symmetry in the hetero-epitaxial $SrIrO_3$ structure [36]. Iridates would continue acting as the profound platform to explore novel physics that may combine the SOC and electron correlations.

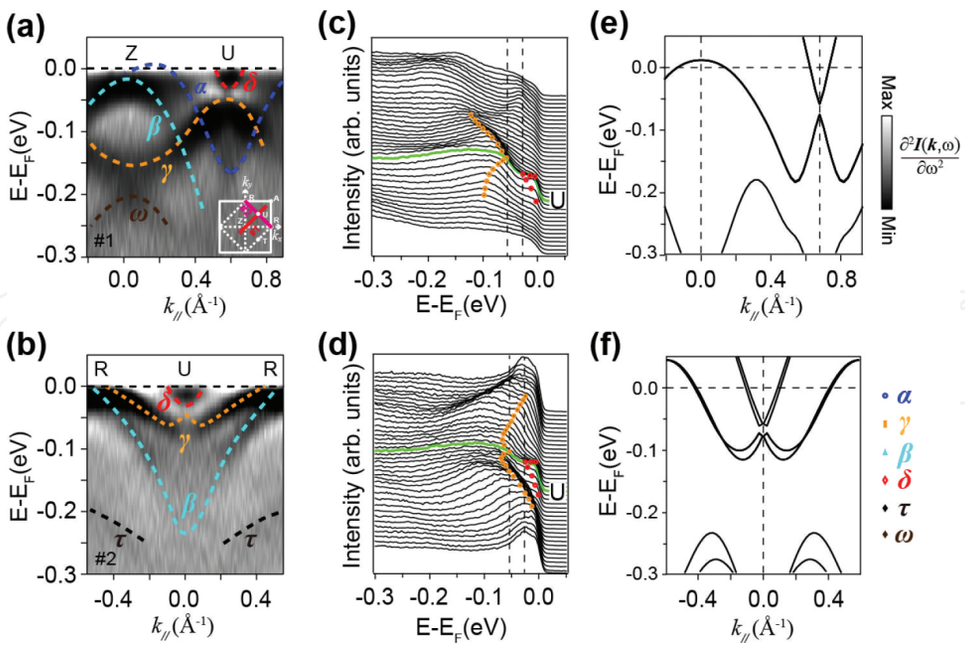

Figure 12. Dirac line node degeneracy lifting around the *U* point of $SrIO_3$. (a) and (b) The second derivative images along *Z*-*U* and *U*-*R* high-symmetry directions, respectively. (c) and (d) The corresponding energy-distribution curves for the photoemission data in (a, b). (e) and (f) The calculated band dispersions along *Z*-*U* and *U*-*R* high-symmetry directions, respectively. Reproduced with permission from Ref. [36].

With the powerful capability of the OMBE-ARPES combo, one can fabricate artificial superlattices which do not exist in nature and study their intriguing emergent physics. Monkman et al. reported the comprehensive investigations on the interfacial electronic structure of $(LaMnO_3)_{2n}/(SrMnO_3)_n$ superlattices as a function of dimensionality [17]. Bulk $LaMnO_3$ and $SrMnO_3$ are anti-ferromagnetic Mott and band insulators, respectively, and $La_{2/3}Sr_{1/3}MnO_3$ is a ferromagnetic metal that exhibits colossal magnetoresistance around its Curie temperature of 370 K. Monkman et al. synthesized high-quality $(LaMnO_3)_{2n}/(SrMnO_3)_n$ superlattices with n = 1–3. Transport studies show that n = 1 and n = 2 members show metallic behaviours at low temperatures, while the n = 3 member exhibits a metal-insulator crossover. **Figure 13** illustrates the evolution of the electronic structure and properties of superlattices upon different n. For n = 1 and 2 members, the Fermi surfaces are apparent and consist of two Mn e_g-derived states: a hole pocket around the Brillouin zone corner, and a smaller electron pocket around the zone centre. For the insulating n = 3 member, the spectral weight at E_F is highly suppressed, although clear states are still observed below E_F. The authors also investigated the near-E_F band dispersions. The n = 1 and 2 members exhibit well-defined and dispersive bands, whereas the n = 3 sample shows only pseudo-gapped intensity at E_F which is similar to polaronic systems with strong electron-phonon coupling. For the critical n = 2, there exists a dramatic difference in electronic states compared to that of n = 1. The states near E_F are substantially suppressed, and a broad incoherent feature appears below E_F, indicating the enhanced correlations. This work provides unique insight into how many-body interactions could be engineered at correlated oxide interfaces, which is an important prerequisite to exploiting such effects in novel electronics [17].

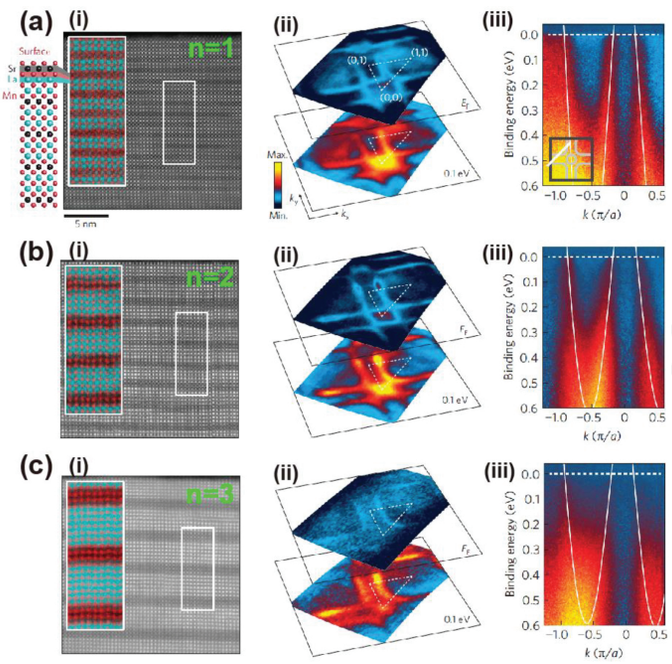

Figure 13. (a)–(c) High-angle annular dark-field scanning transmission electron micrograph (i), Fermi surface (ii) and band dispersion (iii) of $(LaMnO_3)_{2n}/(SrMnO_3)_n$ superlattices with n = 1–3, respectively. Reproduced with permission from Ref. [17].

These examples reflect the powerful capability of the integrated OMBE-ARPES system in studying many-body interactions and resulted novel physics in complex oxides.

5. Conclusion and outlook

In this chapter, we presented the brief inductions to OMBE technique, growth methods and the *in situ* combo integrating oxide MBE and APRES. We demonstrate that OMBE and the *in situ* combo formed with ARPES will continue playing a role in unveiling the intriguing many-body physics of correlated oxide thin films and superlattices as well as exploring novel topological materials in oxide structures.

Author details

Dawei Shen[1,2,3*], Haifeng Yang[1] and Zhengtai Liu[1]

*Address all correspondence to: dwshen@mail.sim.ac.cn

1 State Key Laboratory of Functional Materials for Informatics, Shanghai Institute of Microsystem and Information Technology (SIMIT), Chinese Academy of Sciences, Shanghai, China

2 CAS Centre for Excellence in Superconducting Electronics (CENSE), Shanghai, China

3 CAS-Shanghai Science Research Centre, Shanghai, China

References

[1] P. A. Lee, N. Nagaosa, X. -G. Wen. Doping a Mott insulator: Physics of high-temperature superconductivity. Rev. Mod. Phys. 2006; 78 (1): 17–85.

[2] M. Imada, A. Fujimori, Y. Tokura. Metal-insulator transitions. Rev. Mod. Phys. 1998; 70 (4): 1039–1263.

[3] M. B. Salamon, M. Jaime. The physics of manganites: Structure and transport. Rev. Mod. Phys. 2001; 73 (3): 583–628.

[4] H. Y. Hwang, Y. Iwasa, M. Kawasaki, B. Keimer, N. Nagaosa, Y. Tokura. Emergent phenomena at oxide interfaces. Nat. Mater. 2012; 11 (2): 103–113.

[5] J. Chakhalian, A. J. Millis, J. Rondinelli. Whither the oxide interface. Nat. Mater. 2012; 11 (2): 92–94.

[6] A. Ohtomo, H. Y. Hwang. A high-mobility electron gas at the $LaAlO_3/SrTiO_3$ heterointerface. Nature. 2004; 427 (6973): 423–426.

[7] N. Reyren, S. Thiel, A. D. Caviglia, L.F. Kourkoutis, G. Hammerl, C. Richter,C. W. Schneider, T. Kopp, A. -S. Rüetschi, D. Jaccard, M. Gabay, D.A. Muller, J. -M. Triscone, J. Mannhart. Superconducting interfaces between insulating oxides. Science. 2007; 317 (5842): 1196–1199.

[8] J. H. Lee, L. Fang, E. Vlahos, X. Ke, Y. W. Jung, L. F. Kourkoutis, J. -W. Kim, P. J. Ryan, T. Heeg, M. Roeckerath, V. Goian, M. Bernhagen, R. Uecker, P. C. Hammel, K. M. Rabe, S. Kamba, J. Schubert, J. W. Freeland, D. A. Muller, C. J. Fennie, P. Schiffer, V. Gopalan, E. Johnston-Halperin, D. G. Schlom. A strong ferroelectric ferromagnet created by means of spin-lattice coupling. Nature. 2010; 476 (7358): 954–958.

[9] H. Kroemer. Nobel Lecture: Quasielectric fields and band offsets: teaching electrons new tricks. Rev. Mod. Phys. 2001; 73 (3): 783–793.

[10] A. T. Bollinger, J. Wu, I. Bozovic. Perspective: Rapid synthesis of complex oxides by combinatorial molecular beam epitaxy. APL materials. 2016; 4 (5): 053205.

[11] D. G. Schlom, L. -Q. Chen, X. Q. Pan, A. Schmehl, M. A. Zurbuchen. A thin film approach to engineering functionality into oxides. J. Am. Ceram. Soc. 2008; 91 (8): 2429–2454.

[12] D. G. Schlom. Perspective: Oxide molecular-beam epitaxy rocks! APL materials. 2015; 3 (6): 062403.

[13] A. Damascelli, Z. Hussain, Z. -X. Shen. Angle-resolved photoemission studies of the cuprate superconductors. Rev. Mod. Phys. 2003; 75 (2): 473–541.

[14] A. Damascelli. Probing the electronic structure of complex systems by ARPES. Phys Scripta. 2004; T109: 61–74.

[15] E. J. Monkman, C. Adamo, J. A. Mundy, D. E. Shai, J. W. Harter, D. W. Shen, B. Burganov, D. A. Muller, D. G. Schlom, K. M. Shen. Quantum many-body interactions in digital oxide superlattice. Nat. Mater. 2012; 11 (10): 855–859.

[16] P. D. C. King, H. I. Wei, Y. F. Nie, M. Uchida, C. Adamo, S. Zhu, X. He, I. Bozovic, D. G. Schlom, K. M. Shen. Atomic-scale control of competing electronic phases in ultrathin $LaNiO_3$. Nat. Nanotechnol. 2014; 9 (6): 443–447.

[17] H. C. Xu, R. Peng, D. W. Shen, D. L. Feng. In situ engineering and characterization on the artificial heterostructures of correlated materials with integrated OMBE-ARPES. J. Electr. Spectr. Related Phenom. 2015; 200: 347–355.

[18] A. Y. Cho, J. R. Arthur. Molecular beam epitaxy. Prog. Solid State Chem. 1975; 10 (3): 157–191.

[19] R. A. Betts, C. W. Pitt. Growth of thin-film lithium niobate by molecular beam epitaxy. Electron. Lett. 1985; 21 (21): 960–962.

[20] B. Burganov, C. Adamo, A. Mulder, M. Uchida, P. D. C. King, J. W. Harter, D. E. Shai, A. S. Gibbs, A. P. Mackenzie, R. Uecker, M. Bruetzam, M. R. Beasley, C. J. Fennie, D. G. Schlom, K. M. Shen. Strain control of Fermiology and many-body interactions in two-dimensional Ruthenates. Phys. Rev. Lett. 2016; 116 (19): 197003.

[21] D. L. Proffit, H. W. Jang, S. Lee, C. T. Nelson, X. Q. Pan, M. S. Rzchowski, C. B. Eom. Influence of symmetry mismatch on heteroepitaxial growth of perovskite thin films. Appl. Phys. Letts. 2008; 93 (11): 111912.

[22] N. Nakagawa, H. Y. Hwang, D. A. Muller. Why some interfaces cannot be sharp. Nat. Mater. 2006; 5 (3): 204–209.

[23] J. L. Blok, X. Wan, G. Koster, D. H. A. Blank. Epitaxial oxide growth on polar (111) surfaces. Appl. Phys. Lett. 2011; 99 (15): 151917.

[24] H. F. Yang, Z. T. Liu, C. C. Fan, Q. Yao, P. Xiang, K. L. Zhang, M. Y. Li, J. S. Liu, D. W. Shen. Avoiding polar catastrophe in the growth of polarly orientated nickel perovskite thin films by reactive oxide molecular beam epitaxy. AIP Advs. 2016; 6: 085115.

[25] C. Theis, J. Yeh, D. Schlom, M. Hawley, G. Brown. Adsorption-controlled growth of $PbTiO_3$ by reactive molecular beam epitaxy. Thin Solid Films. 1998; 325 (1C2): 107–114.

[26] J. F. Ihlefeld, A. Kumar, V. Gopalan, D. G. Schlom, Y.B. Chen, X.Q. Pan, T. Heeg, J. Schubert, X. Ke, P. Schiffer, J. Orenstein, L. W. Martin, Y.H. Chu, R. Ramesh. Adsorption-controlled molecular-beam epitaxial growth of $BiFeO_3$. Appl. Phys. Lett. 2007; 91 (7): 071922.

[27] J. H. Lee, X. Ke, R. Misra, J. F. Ihlefeld, X. S. Xu, Z. G. Mei, T. Heeg, M. Roeckerath, J. Schubert, Z. K. Liu, J. L. Musfeldt, P. Schiffer, D. G. Schlom. Adsorption-controlled growth of $BiMnO_3$ by molecular-beam epitaxial. Appl. Phys. Lett. 2010; 96 (26): 262905.

[28] J. Haeni, C. Theis, D. Schlom. RHEED intensity oscillations for the stoichiometric growth of $SrTiO_3$ thin films by reactive molecular beam epitaxy. J. Electroceram. 2000; 4 (2–3): 385–391.

[29] C. M. Brooks, L. F. Kourkoutis, T. Heeg, J. Schubert, D. A. Muller, D. G. Schlom. Growth of homoepitaxial $SrTiO_3$ thin films by molecular-beam epitaxy. Appl. Phys. Lett. 2009; 94 (16): 162905.

[30] J. H. Haeni, C. D. Theis, D. G. Schlom, W. Tian, X. Q. Pan, H. Chang, I. Takeuchi, X. -D. Xiang. Epitaxial growth of the first five members of the $Sr_{n+1}Ti_nO_{3n+1}$ Ruddlesden-Popper homologous series. Appl. Phys. Lett. 2001; 78 (21): 3292–3294.

[31] W. Tian, J. H. Haeni, D. G. Schlom, E. Hutchinson, B. L. Sheu, M. M. Rosario, P. Schiffer, Y. Liu, M. A. Zurbuchen, X. Q. Pan. Epitaxial growth and magnetic properties of the first five members of the layered $Sr_{n+1}Ru_nO_{3n+1}$ oxide series. Appl. Phys. Lett. 2007; 90 (2): 022507.

[32] Y. L. Chen. Studies on the electronic structures of three-dimensional topological insulators by angle resolved photoemission spectroscopy. Front Phys-Beijing. 2012; 7 (2): 175–192.

[33] M. Y. Li, Z. T. Liu, H. F. Yang, J. L. Zhao, Q. Yao, C. C. Fan, J. S. Liu, B. Gao, D. W. Shen, X. M. Xie. Tuning the electronic structure of Sr_2IrO_4 thin films by bulk electronic doping using molecular beam epitaxy. Chin. Phys. Lett. 2015; 32 (5): 057402.

[34] D. E. Shai, C. Adamo, D. W. Shen, C. M. Brooks, J. W. Harter, E. J. Monkman, B. Burganov, D. G. Schlom, K. M. Shen. Quasiparticle mass enhancement and temperature dependence of the electronic structure of ferromagnetic $SrRuO_3$ thin films. Phys. Rev. Lett. 2013; 110 (8): 087004.

[35] H. F. Yang, Z. T. Liu, C. C. Fan, Q. Yao, P. Xiang, K. L. Zhang, M. Y. Li, H. Li, J. S. Liu, D. W. Shen, M. H. Jiang. Origin of the kink in the band dispersion of the ferromagnetic perovskite $SrRuO_3$: electron-phonon coupling. Phys. Rev. B. 2016; 93 (4): 121102(R).

[36] Z. T. Liu, M. Y. Li, Q. F. Li, J. S. Liu, W. Li, H. F. Yang, Q. Yao, C. C. Fan, X. G. Wan, Z. Wang, D. W. Shen. Direct observation of the Dirac node lifting in semimetallic perovskite $SrIrO_3$ thin films. Sci. Rep. 2016; 6: 30309.

[37] Y. Aiura, Y. Yoshida, I. Hase, S. I. Ikeda, M. Higashiguchi, X. Y. Cui, K. Shimada, H. Namatame, M. Taniguchi, H. Bando. Kink in the dispersion of layered strontium ruthenates. Phys. Rev. Lett. 2004; 93 (11): 117005.

[38] Z. Sun, Y. -D. Chuang, A. V. Fedorov, J. F. Douglas, D. Reznik, F. Weber, N. Aliouane, D. N. Argyriou, H. Zheng, J. F. Mitchell, T. Kimura, Y. Tokura, A. Revcolevschi, D. S. Dessau. Quasiparticlelike peaks, kinks, and electron-phonon coupling at the (π,0) regions in the CMR oxide $La_{2-2x}Sr_{1+2x}Mn_2O_7$. Phys. Rev. Lett. 2006; 97 (5): 056401.

[39] S. Aizaki, T. Yoshida, K. Yoshimatsu, M. Takizawa, M. Minohara, S. Ideta, A. Fujimori, K. Gupta, P. Mahadevan, K. Horiba, H. Kumigashira, M. Oshima. Self-energy on the low- and high-energy electronic structure of correlated metal $SrVO_3$. Phys. Rev. Lett. 2012; 109 (5): 056401.

[40] A. Lanzara, P. V. Bogdanov, X. J. Zhou, S. A. Kellar, D. L. Feng, E. D. Lu, T. Yoshida, H. Eisaki, A. Fujimori, K. Kishio, J. -I. Shimoyama, T. Noda, S. Uchida, Z. Hussain, Z. -X. Shen. Evidence for ubiquitous strong electron-phonon coupling in high-temperature superconductors. Nature. 2001; 412 (6846): 510–514.

[41] Y. J. Chang, C. H. Kim, S. -H. Phark, Y. S. Kim, J. Yu, T. W. Noh. Fundamental thickness limit of itinerant ferromagnetic $SrRuO_3$ thin films. Phys. Rev. Lett. 2009; 103 (5): 057201.

[42] M. N. IIiev, A. P. Litvinchuk, H. -G. Lee, C. L. Chen, M. L. Dezaneti, C. W. Chu, V. G. Ivanov, M. V. Abrashev, V. N. Popov. Raman spectroscopy of $SrRuO_3$ near the paramagnetic-to-ferromagnetic phase transition. Phys. Rev. B. 1999; 59 (1): 364.

[43] X. L. Qi, S. C. Zhang. Topological insulators and superconductors. Rev. Mod. Phys. 2011; 83 (4): 1057–1110.

[44] Z. Hasan, C. L. Kane. Colloquium: Topological insulators. Rev. Mod. Phys. 2010; 82 (4): 3045–3067.

[45] D. Xiao, W. Zhu, Y. Ran, N. Nagaosa, S. Okamoto. Interface engineering of quantum Hall effects in digital transition-metal oxide heterostructures. Nat. Commun. 2011; 2 (6): 596.

[46] J. -M. Carter, V. V. Shankar, M. A. Zeb, H. -Y. Kee. Semimetal and topological insulator in perovskite iridates. Phys. Rev. B. 2012; 85 (11): 115105.

[47] M. A. Zeb, H. -Y. Kee. Interplay between spin-orbit coupling and Hubbard interactions in $SrIrO_3$ and related Pbnm perovskite oxides. Phys. Rev. B. 2012; 86 (86): 085149.